Experimenting with machine learning algorithms on quantum computers

Nagy Dániel[1]

[1]Institute for Physics, Eötvös Loránd University, H-1117, Pázmány Péter sétány 1/A. Budapest, Hungary

Created on December 1, 2019

Last update: May 11, 2021

Abstract

A modern számítástechnika jelentős eredményei közé tartozik a gépi tanulás és mesterséges intelligencia alapvető algoritmusainak kifejlesztése és ezek hasznosságának tesztelése különböző feladatokon. Ugyanakkor az elmúlt években a kvantumszámítás is jelentős fejlődésen ment keresztül, olyannyira, hogy 2019-ben a Google kísérleti csapatának sikerült demonstrálnia a kvantumfölényt. A munka során megvizsgáljuk a két terület átfedéséből származó lehetőségeket: klasszikus adatok kvantumos feldolgozását illetve a klasszikus gépi tanulás segítségével történő kvantumos hibajavítást.

Gépi tanulási algoritmusok vizsgálata kvantumszámítógépeken

Nagy Dániel[1]

[1]Eötvös Loránd Tudományegyetem, Fizika Intézet, H-1117, Pázmány Péter sétány 1/A. Budapest, Magyarország

Elkezdve: December 1, 2019

Utolsó frissítés: 2021. május 11.

Kivonat

A modern számítástechnika jelentős eredményei közé tartozik a gépi tanulás és mesterséges intelligencia alapvető algoritmusainak kifejlesztése és ezek hasznosságának tesztelése különböző feladatokon. Ugyanakkor az elmúlt években a kvantumszámítás is jelentős fejlődésen ment keresztül, olyannyira, hogy 2019-ben a Google kísérleti csapatának sikerült demonstrálnia a kvantumfölényt. A munka során megvizsgáljuk a két terület átfedéséből származó lehetőségeket: klasszikus adatok kvantumos feldolgozását illetve a klasszikus gépi tanulás segítségével történő kvantumos hibajavítást.

[Dani: Acknowledgement]

Contents

List of Figures

1 Introduction

Quantum computing is probably the most promising emerging technology with many possible applications across all domains of science and business. The idea of quantum computing was first proposed by Richard P. Feynman as a method to simulate quantum mechanics. Since the size of the Hilbert-space grows exponentially with the complexity of the quantum system, and thus the calculations become intractable on any classical computer, Feynmans idea was to simulate quantum physics on devices that behave themselves according to the rules of quantum physics.

Soon after Feynmans proposal, scientists became to establish the theoretical background of quantum information and quantum computing. Some of the quantum algorithms are proven to have an advantage over any known classical algorithm. One of the first such quantum algorithm is the Deutsch-Jozsa algorithm [2], which decides if a binary function f is balanced or constant. Probably the most notable quantum algorithm was proposed by Peter W. Shor in 1994, which is a polynomial-time quantum algorithm for factoring large integers [3]. This is the first quantum algorithm with a real-life application, because most of the public-key cryptosystems could be broken with an efficient algorithm for integer factoring. Another important quantum algorithm is the Grover's algorithm proposed by Lov K. Grover in 1996 for searching an unordered database [4]. While the best known classical algorithm for searching unordered databases runs in $O(N)$ time, Grover's algorithm solves this problem with $O(\sqrt{N})$ oracle queries. Beyond quantum algorithms, many quantum-inspired algorithms were discovered [5, 6, 7].

2 Quantum Computing with continuous variables

[Dani: cite: Xanadu paper, Photonic Supremacy paper, PsiQuantum Fusion-Based QC]
Continuous variable (CV) systems have infinite degrees of freedom, and therefore the corresponding Hilbert-space is of infinite dimensions. Such systems can be modeled by M harmonic oscillators, which are usually called *modes*. With H_k denoting the Hilbert-space of the kth mode, the Hilbert-space of the full CV system is their direct sum:

$$\mathcal{H} = \bigoplus_{k=1}^{M} \mathcal{H}_k. \tag{1}$$

The Hamiltonian of mode j can be described by introducing bosonic creation and annihilation operators $a_j^\dagger$ and a_j, obeying the following canonical commutation relations:

$$\left[\hat{a}_j, \hat{a}_k^\dagger\right] = \delta_{jk}, \left[\hat{a}_j^\dagger, \hat{a}_k^\dagger\right] = [\hat{a}_j, \hat{a}_k] = 0. \tag{2}$$

The effect of the creation and annihilation operators on the Fock space can be described by the following identities:

$$\begin{aligned} \hat{a}_k^\dagger \left|n_1, \ldots, n_k, \ldots\right\rangle &= \sqrt{1+n_k} \left|n_1, \ldots, n_k + 1, \ldots\right\rangle \\ \hat{a}_k \left|n_1, \ldots, n_k, \ldots\right\rangle &= \sqrt{n_k} \left|n_1, \ldots, n_k - 1, \ldots\right\rangle \end{aligned} \tag{3}$$

We also introduce the number operator $\hat{n}_j = \hat{a}_j^\dagger \hat{a}_k$:

$$\hat{a}_k^\dagger \hat{a}_k |n_1, ..., n_k, ...\rangle = \hat{n}_k |n_1, ..., n_k, ...\rangle = n_k |n_1, ..., n_k, ...\rangle \tag{4}$$

Each of the single-mode Hilbert-space $\mathcal{H}_k$ is an infinite-dimensional Fock-space spanned by the eigenvectors of the number operator $\hat{n}_k = \hat{a}_k^\dagger \hat{a}_k$ labeled $\{|n\rangle\}_k$. It is often useful to introduce the canonical position operators X_j and momentum operators P_j which are related to the creation and annihilation operators by the following transformations:

$$\hat{X}_k = \frac{\hat{a}_k + \hat{a}_k^\dagger}{\sqrt{2}} \qquad \hat{a}_k = \frac{\hat{X}_k + i\hat{P}_k}{\sqrt{2}} \tag{5}$$

$$\hat{P}_k = \frac{\hat{a}_k - \hat{a}_k^\dagger}{i\sqrt{2}} \qquad \hat{a}_k^\dagger = \frac{\hat{X}_k - i\hat{P}_k}{\sqrt{2}} \tag{6}$$

Operators $\hat{X}_k$ and $\hat{P}_k$ are called quadrature operators. Following the notation often used in literature, we group these operators into a vector

$$\mathbf{R}^\top = (\hat{X}_1, \hat{P}_1, \hat{X}_2, \hat{P}_2, ..., \hat{X}_k, \hat{P}_k, ..., \hat{X}_M, \hat{P}_M) \tag{7}$$

We can calculate the commutators $[\mathbf{R}_k, \mathbf{R}_l]$ by introducing a symplectic form $\boldsymbol{\Omega}$ as

$$\boldsymbol{\Omega} = \bigoplus_{j=1}^{M} \boldsymbol{\omega},\ \boldsymbol{\omega} = \begin{pmatrix} 0 & 1 \\ -1 & 0 \end{pmatrix}. \tag{8}$$

Using this notation, we can write

$$[\mathbf{R}_k, \mathbf{R}_l] = i\boldsymbol{\Omega}_{kl} \tag{9}$$

Apart from the Fock-basis, there is another useful alternative basis, the basis of *coherent states*, which are eigenstates of the annihillation operator $\hat{a}_k$:

$$\hat{a}_k |\alpha\rangle_k = \alpha |\alpha\rangle_k, \tag{10}$$

with $\alpha \in \mathbb{C}$. From definition this, we can derive that the Fock-basis expansion of the coherent state $|\alpha\rangle_k$ is

$$|\alpha\rangle_k = e^{-\frac{1}{2}|\alpha|^2} \sum_{n=1}^{\infty} \frac{\alpha^n}{\sqrt{n!}} |n\rangle_k. \tag{11}$$

The derivation of the above formula is explained in detail in appendix A. By introducing the single-mode Weyl-displacement operator

$$\hat{D}_k(\alpha) = e^{\alpha \hat{a}_k^\dagger - \alpha^* \hat{a}_k}, \tag{12}$$

we can create coherent states from the vacuum state: $|\alpha\rangle_k = \hat{D}_k(\alpha) |0\rangle_k$. Of course, we can define multimode coherent states

$$|\alpha_1\rangle_1 \otimes |\alpha_2\rangle_2 \otimes \cdots \otimes |\alpha_N\rangle_N \equiv |\boldsymbol{\xi}\rangle = \hat{D}(\boldsymbol{\xi}) |0\rangle, \tag{13}$$

where $\hat{D}(\boldsymbol{\xi})$ is the multi-mode Weyl-displacement operator defined as

$$\hat{D}(\boldsymbol{\xi}) = e^{i\mathbf{R}^\top \boldsymbol{\Omega} \boldsymbol{\xi}}, \ \boldsymbol{\xi} \in \mathbb{R}^{2N}. \tag{14}$$

For a single mode,

$$\hat{D}_k(\boldsymbol{\xi}) = \hat{D}_k \begin{pmatrix} \xi_1 \\ \xi_2 \end{pmatrix} = e^{i(\xi_2 \hat{X}_k - \xi_1 \hat{P}_k)}, \text{ if we set } \begin{pmatrix} \xi_1 \\ \xi_2 \end{pmatrix} = \frac{1}{\sqrt{2}} \begin{pmatrix} \mathrm{Re}(\alpha_k) \\ \mathrm{Im}(\alpha_k) \end{pmatrix} \tag{15}$$

[Dani: Write about phase-space, quasiprobability] [Dani: Write about different quantum gates.] [Dani: Write about homodyne measurements, heterodyne measurements and photon number-resolving measurements]

3 Machine learning

Machine learning is simply said, a new paradigm in software development. Traditional software have a predefined behaviour, which does not change over time. In contrast, machine learning models are iteratively "trained" i.e. updated to achieve better performance by the use of data. These algorithms are designed to learn patterns from the data available and update themselves with new experience. Although, there are a lot of machine learning algorithms, they usually fit into one of the following three main classes:

- **Supervised Learning**. Supervised Learning (SL) algorithms need labeled data, and based on the input-output pairs previously seen by the algorithm, it learns to produce correct outputs for previously unseen inputs. A very basic example of supervised learning is the linear regression or support vector machines **[Dani: ref?]** for classification, but there are a lot of complex models like CNNs for image classification **[Dani: ref?]**, which are trained in a supervised manner.
- **Unsupervised Learning**. Unsupervised Learning (UL) does not require labeled data, instead of that, it is trying to learn from a lot of unlabeled data points. These algorithms include a bunch of clustering methods, like k-means **[Dani: ref?]**, or mixture models **[Dani: ref?]**. Another example of unsupervised learning is latent variables or distributions for feature extraction or data denoising. A great example of latent distribution learning are Variational Autencoders [8] which have bean adobted for a variety of tasks.
- **Reinforcement Learning**. Reinforcement Learning (RL) is very different from the previously mentioned two classes of machine learning method. In RL the goal is not to learn from a given set of data, but rather to solve a specific task in an environment. In RL, an *agent* learns to perform a task by observing the state (or some subspace of the state) of the surrounding environment, and executing actions in order to maximize an objective. RL is inspired by the process of learning from mistakes or rewards. The environment in RL can be any type of physical simulation, or even a computer game. Examples for RL algorithms include Deep Q-networks [9] or AlphaGo [10]

3.1 Supervised Classification and Regression

The two most common SL tasks are **classification** and **regression**. Both classification and regression can be performed with traditional algorithms or deep neural networks. In this chapter we present the basic ideas and formalisms of classification and regression which will be useful in the following chapters.

In supervised learning the data points consist of pairs $(\mathbf{x}_i, \mathbf{y}_i)$, where $\mathbf{x}_i$ are called feature vectors and $\mathbf{y}_i$ are called labels. Both the feature vectors and the labels are real-valued vectors of any dimension. Feature vectors can be pre-processed to achieve better performance. A dataset is usually split into two or three parts. The first part is usually the largest, which is called the training set, and this is used to train the model. The second dataset is called testing or evaluation set and is used to evaluate how the model performs when it is fed with previously unseen data. There might be an additional set called the validation set, which is used to verify the model's performance after training is finished. While the testing set is used to monitor the learning process during training, the validation set is used only after the full training process is finished.

3.1.1 Classification

In classification, each point $\mathbf{x}$ is in one of K predefined categories. That is, the labels are integers less or equal to K: $y_i \in \{1, ..., K\}$. The goal of a classifier is to learn the connection between $\mathbf{x}_i$ and y_i, in other words, to learn, how to put each vector $\mathbf{x}_i$ into the right category. The performance of a classifier is usually measured with categorical accuracy i.e. what percentage of the predicted labels are in the right category. Apart from accuracy, it is often useful to introduce the categorical cross-entropy. In general, the crossentropy of two probability distributions p and q is defined as

$$H(p, q) = -\int p(x) \log q(x) \mathrm{d}x \tag{16}$$

[Dani: Explain the intuition behind entropy, cross-entropy etc.] To transform this general formula of cross-entropy to the case of classification, we need to introduce one-hot encoding. One-hot encoding maps integer labels to binary vectors in a way that vector corresponding to the label j will contain 1 at the jth position and 0 everywhere else. The length of the resulting vectors is K. For example the one-hot encoding of labels 1 and 3 in case of three categories would look like

$$\texttt{OneHot}(1, 3) = \begin{bmatrix} 1 \\ 0 \\ 0 \end{bmatrix} \qquad \texttt{OneHot}(3, 3) = \begin{bmatrix} 0 \\ 0 \\ 1 \end{bmatrix} \tag{17}$$

In machine learning, especially in deep learning one-hot encoding of categorical features or labels is proven to be very useful. Now, with one-hot encoded labels, we can easily define the categorical crossentropy:

$$\texttt{CrossEntropy} : \mathbb{R}^K \times \mathbb{R}^K \to \mathbb{R},\ \texttt{CrossEntropy}(\mathbf{y}^{\text{pred}}, \mathbf{y}^{\text{true}}) = -\sum_{i=1}^{K} y_i^{\text{true}} \log y_i^{\text{pred}} \tag{18}$$

The crossentropy essentially measures how the predicted distribution of labels differs from the true distribution, hence it is widely used in machine learning. Applications of classification include image recognition, image segmentation, speech and voice recognition, fraud detection and a lot more.

3.1.2 Regression

Regression models are usually used for forecasting and prediction, or simply to uncover the relationships between two or more features. Opposed to classification, in regression, the output of the model is not restricted to a discrete set of predefined classes, instead the set of possible outputs is a bounded or unbounded subset of $\mathbb{R}^d$. Therefore, classification is a special case of regression where the set of possible values of the outcomes is a finite set of integers. Apart from this difference, the purpose of regression is the same: to find a connection between the features $\mathbf{x}$ and labels $\mathbf{y}$. The elements of feature vectors x_i are usually called independent variables or predictors, while the elements of the label vectors y_i are called dependent variables. Formally the regression model is a function approximator, which is itself a function that can be parametrized by a set of real parameters $\boldsymbol{\theta} \in \mathbb{R}^m$. Given a set of observations $\{(\mathbf{x}_1, y_1), (\mathbf{x}_2, y_2), ...(\mathbf{x}_N, y_N)\}$ a function approximator $f(\cdot; \boldsymbol{\theta})$, we can write

$$y_i = f(\mathbf{x}_i; \boldsymbol{\theta}) + \epsilon_i, \tag{19}$$

Where ϵ_i denotes a random statistical noise, usually assumed to follow Gaussian distribution. The goal is to find an optimal set of parameters $\boldsymbol{\theta}^*$ which minimizes the mean squared error:

$$\boldsymbol{\theta}^* = \arg\min_{\boldsymbol{\theta}} \sum_{k=1}^{N} (y_k - f(\mathbf{x}_k; \boldsymbol{\theta}))^2 \tag{20}$$

The mean squared error is itself a good measure of the performance of the regression model and is often used in machine learning and deep learning. Another scalar value for getting some information about the goodness of fit is the coefficient of determination or often called R^2-score. The R^2-score is a real value usually falling between zero and one (the latter meaning perfect fit), although sometimes it can be negative. The R^2-score measures the proportion of variance in the predictions that can be explained by the data. To calculate the R^2-score, we first introduce the total sum of squares

$$SS_{\text{tot}} = \sum_i (y_i^{\text{true}} - \langle y^{\text{true}} \rangle)^2, \tag{21}$$

where $\langle y^{\text{true}} \rangle = \frac{1}{N} \sum_k y_k^{\text{true}}$ is the mean of the dependent variable in the dataset. Then we calculate the sum of squared residuals, or sum of squared errors:

$$SS_{\text{res}} = \sum_i (y_i^{\text{true}} - y_i^{\text{pred}})^2. \tag{22}$$

With these two quantities, we can now define the R^2-score as follows:

$$R^2 = 1 - \frac{SS_{\text{res}}}{SS_{\text{tot}}}. \tag{23}$$

3.2 Deep Neural Networks and backpropagation

Probably the most successful machine learning models are deep neural networks, which enjoy a great popularity in the recent years because of their flexibility and expressive power [11]. In this chapter we give a short introduction to deep neural networks by descibring the basic ideas behind training neural networks for various tasks.

Human brain is very good at some tasks in which computers are quite bad. While a computer can calculate that $567,213 \times 789,133 = 447,606,496,329$ in a few milliseconds it can not decide wheter a picture shows a dog or a cat. In contrary humans are very good at recognizing pictures and deciding wheter a picture shows a dog or a cat takes less than a second for a brain. Therefore the idea to mimic the brain with computers and solve tasks with brain-like algorithms seems plausible. Although the basic idea is very simple, it took scientists decades to make practically useful neural networks and training neural networks still requires huge amounts of computational power. To mimic the neural network of the brain, we need to come up with a mathematical model that is simple enough to be simulated on computers, but still complex enough to be able to learn how to do difficult tasks. Not surprisingly each neuron will be modeled by a parametric function $g(\mathbf{x}; \mathbf{W}, \mathbf{b})$. Before defining the function g explicitly we should review, how biological neurons work.

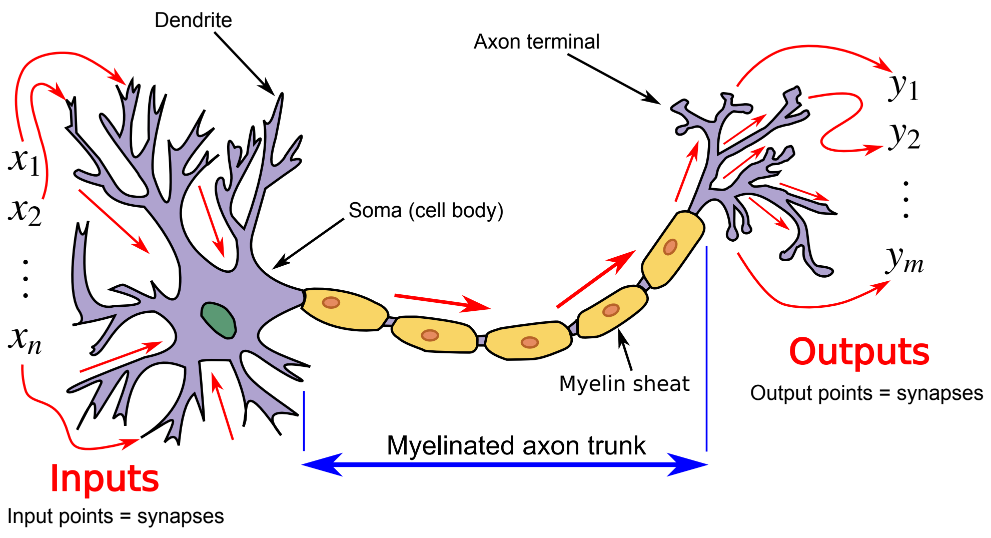

Figure 1. neuron from [1]

Figure 1 shows a biological neuron with input and output synapses. Each of the input and output synapses is connected to other cells forming the neural network with billions of individual cells. Without diving into the biochemical details, we can say that information is carried down the axon in the form of spike-like electric pulses, and transmitted through the synapse with the help of ions neurotransmitters and positive ions. The electrical potential in the cells is typically -70mV. When a synapse receives a signal, this potential slightly increases, and when it reaches a treshold of ≈ -55mV, the cell fires, and a signal will be sent to the output synapses. Different input synapses have different importance, and thus they contribute to the output signal with different coefficients. Therefore, we can say that the output frequency of the i-th neuron is modeled by

$$y_i = \theta\left(\sum_j J_{ij} x_j - U_0\right), \tag{24}$$

where $\theta(x)$ is the Heaviside-step function, x_j are input frequencies and $U_0 = -55$mV is the treshold potential. From this model, we can derive a more general neuron model, which will be used to train deep neural networks:

$$\mathbf{y} = g\left(\mathbf{W}^\top \mathbf{x} + \mathbf{b}\right), \tag{25}$$

where g is called *activation function*, $\mathbf{W}$ and $\mathbf{b}$ are the *weights* and *bias*es, respectively. Some commonly used activation functions are shown on figure 3 This model of a single neuron is called a perceptron. The simplest form of deep neural network uses many perceptrons and is called a *multilayer-perceptron* (MLP), see figure 2. In this case the input vectors are fed into many perceptrons, and the outputs of these is fed into the perceptrons of the next layer. This architecture is often called fully connected or dense neural network, and the layers of perceptrons are called hidden layers. The outputs of an MLP can be scalars vector, or in some cases tensors of higher rank.

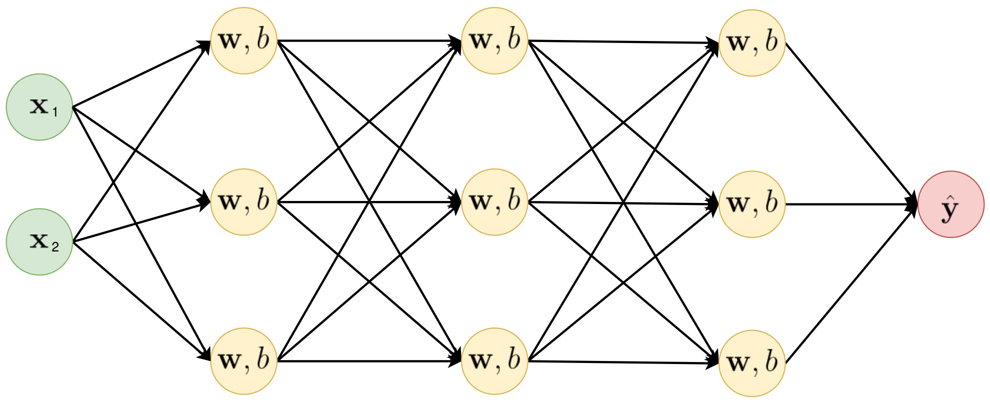

Figure 2. The multilayer perceptron architecture. Green circles are the input features which can be scalar or vector values, the yellow circles represent the weights and biases of the perceptrons of the hidden layers, while the red circle is the output. Data flow is noted with black arrows.

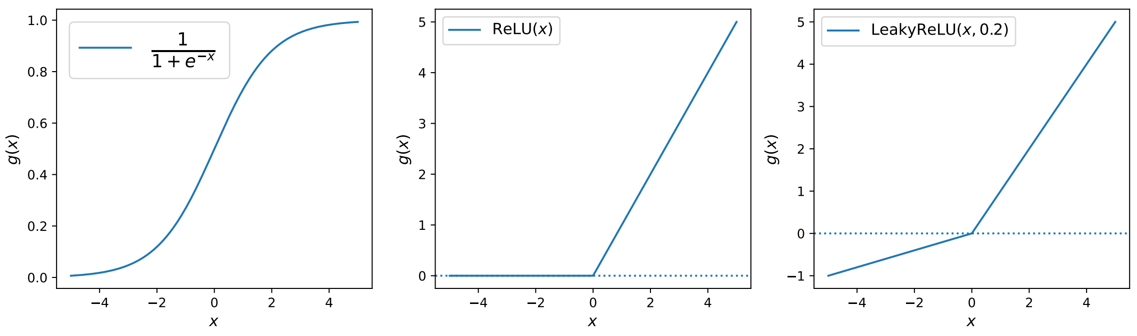

Figure 3. The three most frequently used activation functions in deep neural networks. Left: the sigmoid function, middle: rectified linear unit (ReLU), right: leaky ReLU.

There are many more sophisticated neural network architectures like convolutional neural networks (CNNs) [12], which are useful for image processing tasks, recursive neural networks with internal long term memory [13] for speech recognition or time-series forecasting, or transformers [14] for machine translation. To dive into the details of these complex deep neural network architectures is out of the scope of this thesis. We will, however explain the gradient descent (GD) algorithm, which makes it possible to train complex neural networks with the help of automatic differentiation. The training of deep neural networks for various machine learning task became possible after the proposal of backpropagation algorithm in 1986 by Geoffrey Hinton et. al. [15]. Essentially, training neural networks is finding the best weights $(\mathbf{W}^*, \mathbf{b}^*) \equiv \boldsymbol{\theta}^*$, for which a defined loss function $\mathcal{L}$ has minimum:

$$\boldsymbol{\theta}^* = \arg\min_{\boldsymbol{\theta}} \mathcal{L}(\mathbf{y}, f(\mathbf{x}; \boldsymbol{\theta})), \tag{26}$$

where $f(\cdot;\boldsymbol{\theta})$ represents the neural network. The idea of gradient descent is to find $\boldsymbol{\theta}^*$ by starting at a random point $\boldsymbol{\theta}^{(0)}$ and at each timestep update theta in the direction of gradient. In the standard version of gradient-descent, we calculate the average loss $L = \frac{1}{N}\sum_{k=1}^{N} \mathcal{L}(\mathbf{y}_k, f(\mathbf{x}_k; \boldsymbol{\theta}^{(t)}))$ for the entire dataset to do a single step of gradient descent (see algorithm 1).

Algorithm 1 Gradient Descent

```
1: procedure GradientDescent($\{(\mathbf{x}_k, \mathbf{y}_k)\}_{k=1}^{N}$, $f$, $\boldsymbol{\theta}^{(0)}$, $\mathcal{L}$, $\alpha^{(0)}$, $T$)
2:     for all $t \in \{0, ..., T\}$ do
3:         Calculate $L = \frac{1}{N}\sum_{k=1}^{N} \mathcal{L}(\mathbf{y}_k, f(\mathbf{x}_k; \boldsymbol{\theta}^{(t)}))$
4:         for all $\theta_j \in \boldsymbol{\theta}$ do
5:             Calculate the gradients $\left.\frac{\partial L}{\partial \theta_j}\right|_{\theta_j=\theta_j^{(t)}}$
6:             Update the parameter $\theta_j^{(t+1)} \leftarrow \theta_j^{(t)} - \alpha_j^{(t)} \left.\frac{\partial L}{\partial \theta_j}\right|_{\theta_j=\theta_j^{(t)}}$
7:         end for
8:     end for
9: end procedure
```

In many cases, the dataset is very large, and it turned out to be useful to split the dataset into mini-batches of a small size and calculate the losses and gradients for each individual min-batch. This version of gradient descent is called mini-batch stochastic gradient descent or mini-batch SGD, sometimes simply SGD. Using SGD instead of GD not only improves the overall perform ance of the models, but usually reduces time needed for convergence.

$$\texttt{Softmax} : \mathbb{R}^m \to \mathbb{R}^m, \ [\texttt{Softmax}(\mathbf{x})]_j = \frac{e^{x_j}}{\sum\limits_k e^{x_k}} \tag{27}$$

4 Quantum Machine Learning

QSVM paper = [16] HHL paper = [17] Feature Hilbert Spaces = [18]

[Dani: related papers: quantum svm, Kernel methods, HHL algorithm for matrix inversion, quantum-inspired classical algos
motivation: summary from Lloyd paper, regression, classification, hybrid traning, encoding, inference
General structure: encoding, rotations and beamsplitter = interferometer, squeezing, interferometer, displacement, all = affine transformation + at the end non-linear, e.g., cubic phase operation (numeric instability switch to Kerr gates –> write at the performance test)
Loss functions: regression, classification
Regularization: keep trace close to zero, non-Gaussian
]

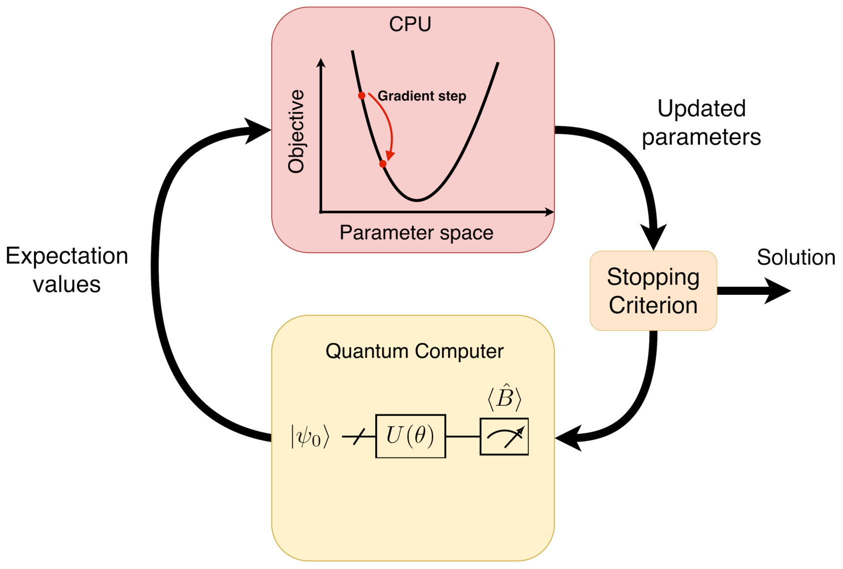

Figure 4. VQC-optimization.

4.1 Variational Quantum Eigensolver

Variational Quantum Eigensolvers [19] are hybrid quantum-classical algorithms designed to find the lowest energy eigenvalue of some Hamiltonian H. VQEs are one of the most studied quantum algorithms because of their expected use cases in quantum chemistry and materials science [20, 21, 22, 23]. VQEs are a special class of variational quantum circuits, where the operator being measured is the Hamiltonian of some system. The basic idea behind the variational quantum eigensolver is as follows. First we fix the structure of a parametric quantum circuit called the ansatz, defined by a unitary $U(\boldsymbol{\theta})$, where $\boldsymbol{\theta} \in \mathbb{R}^m$ are real parameters. Then we start by some initial state $|\psi_0\rangle$, which is usually $|0\rangle^{\otimes M}$ in the qubit setting. For the continuous variable setting, the initial state can be the vacuum state, a displaced state, a squeezed state, or a photon number eigenstate. After preparing the circuit, we evaluate the expectation value of the Hamiltonian which is eventually the cost, or loss:

$$\mathcal{L}(\boldsymbol{\theta}) = \langle H \rangle = \langle\psi_0| U^\dagger(\boldsymbol{\theta}) H U(\boldsymbol{\theta}) |\psi_0\rangle \tag{28}$$

The goal is to minimize the loss $\mathcal{L}$ by iteratively updating the parameters $\boldsymbol{\theta}$ with some update rule. This update rule can be any gradient-free [24] or gradient-based method **[Dani: idezet]**. To use gradient descent optimization in the VQE setting, we need to evaluate the gradient $\nabla_{\boldsymbol{\theta}}\mathcal{L}$, which can be challenging, and is described in details in chapter 4.3. Algorithm 2 describes the variational quantum eigensolver with a general gradient-based learning method. Notice that we wrote $\alpha_j^{(t)}$ for the learning rate, since in most modern optimizers like Adam [25], each parameter has its own learning rate and it may depend on the number of iterations already done.

Algorithm 2 K-shot VQE

```
 1: procedure K-VQE($H, K, T, \alpha$)
 2:     for all $t \in \{1, ..., T\}$ do
 3:         Prepare the ansatz $U(\boldsymbol{\theta})$
 4:         Estimate the loss $\mathcal{L} = \langle\psi_0| U^\dagger(\boldsymbol{\theta}) H U(\boldsymbol{\theta}) |\psi_0\rangle$ by averaging $K$ shots
 5:         for all $\theta_j \in \boldsymbol{\theta}$ do
 6:             Calculate the quantum gradient $\partial_{\theta_j}\mathcal{L}$
 7:             Update the parameter $\theta_j \leftarrow \theta_j - \alpha_j^{(t)}\partial_{\theta_j}\mathcal{L}$
 8:         end for
 9:     end for
10: end procedure
```

4.2 Quantum Neural Networks

Cv-Qnns -LLoyd = [26]

4.3 Calculating the gradients of the parameters

In this section, we introduce the theory of calculating quantum gradients in the continuous variable setting. We follow the notation of Shuld et. al. [27]. A variational quantum circuit is defined by a unitary $U(\boldsymbol{\theta})$, $\boldsymbol{\theta} \in \mathbb{R}^m$, an initial state $|\psi_0\rangle$ and a measurment operator B. We can understand a variational citcuit as $f : \mathbb{R}^m \to \mathbb{R}$, **[Dani: The Schuld paper writes $f : \mathbb{R}^m \to \mathbb{R}^n$, maybe a typo???]** which maps the circuit parameters to the expectation value of operator B:

$$f(\boldsymbol{\theta}) = \langle\psi_0| U^\dagger(\boldsymbol{\theta}) B U(\boldsymbol{\theta}) |\psi_0\rangle \tag{29}$$

In gradient-based optimizations, we need the gradient $\nabla_{\boldsymbol{\theta}} f$, and this eventually means calculating the partial derivatives $\partial_\mu f$, $\mu \in \boldsymbol{\theta}$. In the continuous variable setting, observables are usually polynomials of the quadrature operators X_j and P_j.

5 Results

In this chapter we present the results of our numerical experiments. In section 5.2 we present the results obtained by applying a CV QNN to some regression tasks, in section 5.1 we discuss the performance of the QNN-s on various classification examples. Finally, in section 5.3 we present the performance of a continuous-variable VQE on finding the ground-state energy of a Bose-Hubbard model. These numerical experiments were run using Strawerry Fields [28, 29], an open-source software for simulating photonic quantum circuits an Tensorflow [30], Google's open-source framework for calculating gradients via automatic differentiation. Although these software packages are very powerful and efficient for computing matrix algebra and simulating quantum circuits, due to the exponential scaling of the Hilbert-space of CV quantum systems, we can not efficiently simulate quantum circuits with more then a few qumodes. Therefore, in the regression and classification example we use only two qumodes with cutoff dimension 10, while in the VQE setting we used four qumodes with cutoff dimension 5.

5.1 Classification

In this section we present the architecture we used to solve different classification tasks using quantum neural networks and of course we present the results as well. We tested the same ansatz circuit with the same loss function on three different synthetic datasets: blobs, moons and circles (see figure 6 a-c). The datasets are generared with scikit-learn [31], a python package which contains a lot of implementations of data preprocessing and machine learning algorithms. We use an Ansatz circuit architecture inspired by [26], composed of beamsplitters, displacment and squeezing gates and Kerr nonlinearities. Figure 5 shows the ansatz circuit with a single layer.

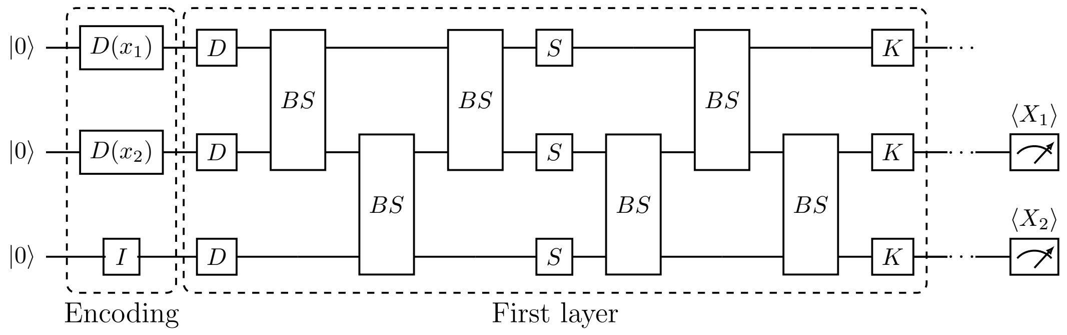

Figure 5. Ansatz circuit used in the classification task with the first layer.

In all three datasests we used, the feature vectors are two-dimensional spacial coordinates $\mathbf{x} = (x_1, x_2)$, and we use displacement encoding to encode these vectors into quantum states. We use three-mode quantum neural network, and therefore the encoding function is

$$(x_1, x_2) \mapsto \hat{D}_1(x_1) \otimes \hat{D}_2(x_2) \otimes I_3 \left|0, 0, 0\right\rangle , \tag{30}$$

and we can decompose $\hat{U}(\mathbf{x}; \boldsymbol{\theta})$

$$\hat{U}(\mathbf{x}; \boldsymbol{\theta}) = \hat{U}'(\boldsymbol{\theta}) \otimes \left(\hat{D}_1(x_1) \otimes \hat{D}_2(x_2) \otimes I_3\right) . \tag{31}$$

To construct the loss function, we use homodyne measurements with `Softmax` and `CrossEntropy`. Depending on the number of classes in the dataset we measure modes $1-3$ in the case of blobs or $2-3$ in the case of moons and circles. The loss is simply

$$\mathcal{L} = \texttt{CrossEntropy}(\mathbf{y}^{\text{pred}}, \mathbf{y}^{\text{true}}) + \frac{\lambda}{|\mathcal{B}|} \sum ||W^{\text{active}}||^2, \tag{32}$$

where

$$\mathbf{y}^{\text{pred}} = \texttt{Softmax} \begin{bmatrix} \text{abs}\left(\text{Tr}\left[\hat{\rho}\hat{X}_1\right]\right) \\ \text{abs}\left(\text{Tr}\left[\hat{\rho}\hat{X}_2\right]\right) \\ \text{abs}\left(\text{Tr}\left[\hat{\rho}\hat{X}_3\right]\right) \end{bmatrix} \text{ or } \mathbf{y}^{\text{pred}} = \texttt{Softmax} \begin{bmatrix} \text{abs}\left(\text{Tr}\left[\hat{\rho}\hat{X}_2\right]\right) \\ \text{abs}\left(\text{Tr}\left[\hat{\rho}\hat{X}_3\right]\right) \end{bmatrix}, \tag{33}$$

and W^{active} are the weigths of the active gates in the QNN. This way, assuming that the output state of the QNN is pure, we can write

$$\rho = |\psi\rangle\langle\psi| \text{ with } |\psi\rangle = \hat{U}(\mathbf{x}; \boldsymbol{\theta}) \left|\psi_0\right\rangle . \tag{34}$$

In most cases this assumption is true in our simulations, because we use L^2 normalization on the active weights of the network, and thus $\text{Tr}\left[\rho^2\right] \approx 1$.

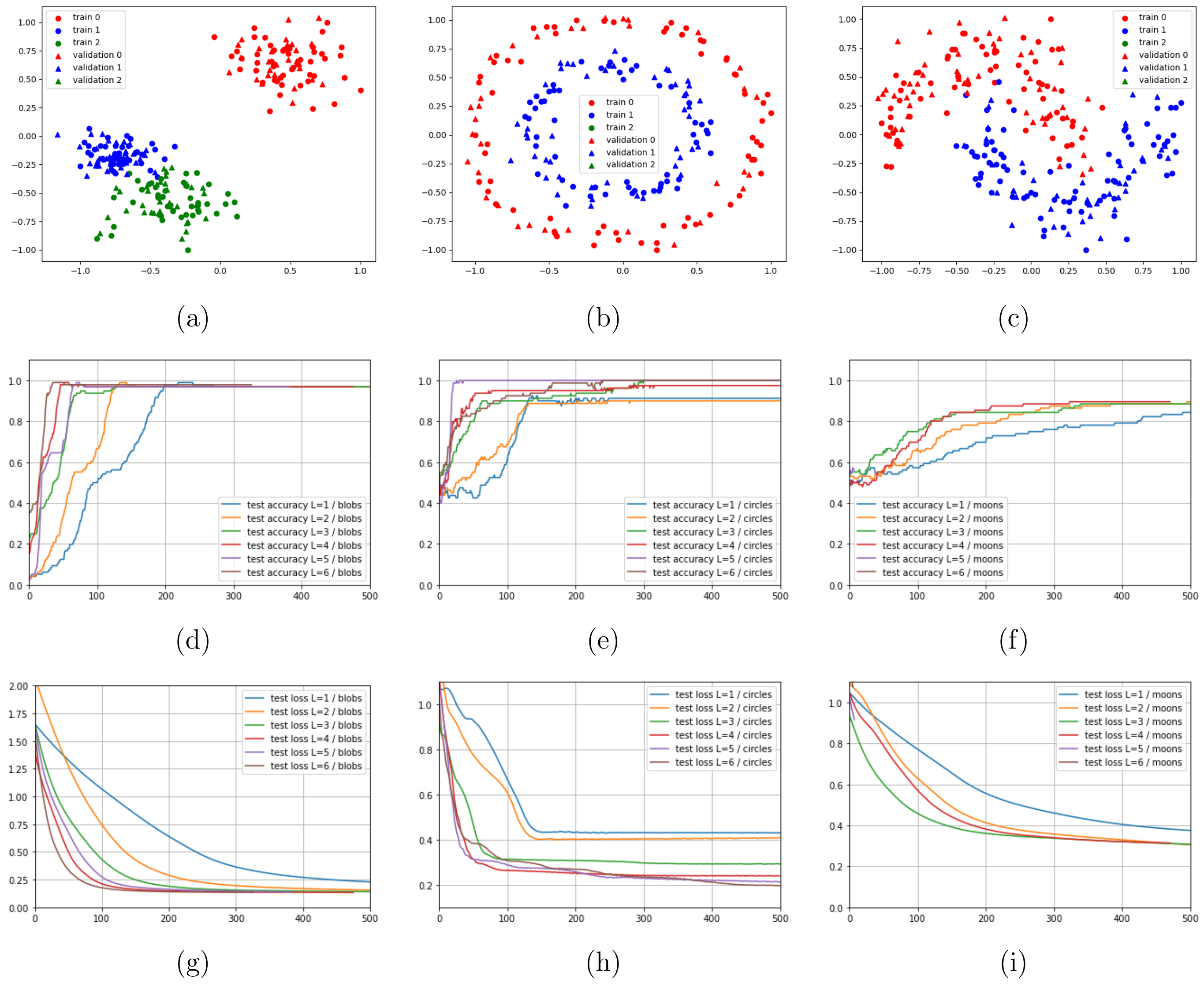

Figure 6. leiras

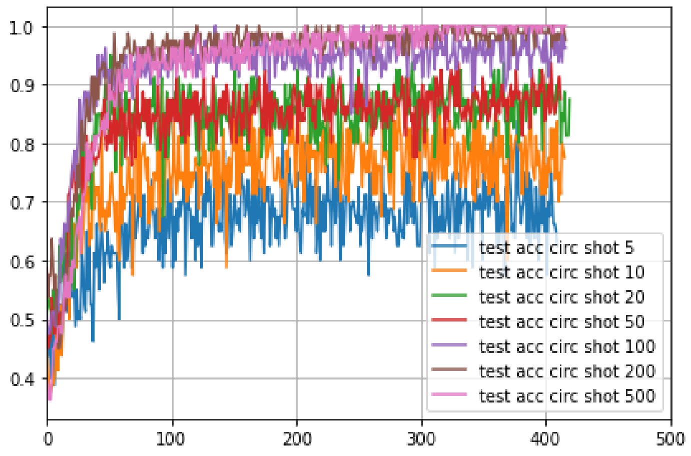

Figure 7.

5.2 Regression

As specified earlier, the aim of regression is to predict or forecast a value y for previously unseen feature vectors $\mathbf{x}$ by inferring a function f from given example pairs $(\mathbf{x}_k, y_k)$. In this chapter, we present our results on testing regression with parametric quantum circuits on a photonic CV architecture. We test our methods on synthetic datasets, as well as on a real-world dataset. In the simulations presented hereby, both the feature and the dependent value are scalars. **[Dani: Data normalization and encoding]** Data normalization is usually a very important step in order to achieve good performance in machine learning. Therefore, we normalized our datasets so that most of the x and y values fall into the $[-1, 1]$ interval. In chapter 4.2 we saw that encoding classical data into a quantum state is a crucial step in quantum machine learning. Therefore we tested different encodings and found that displacement encoding works the best in each of the simulations. Hence, in all of the simulations presented in this thesis we use displacement encoding, which means that the feature x is encoded into the quantum system by applying a single-mode Weyl-displacement operator $\hat{D}(x)$ on one or more modes. In the regression task, we apply the same displacement on all of the modes:

$$x \mapsto \hat{D}_1(x) \otimes \hat{D}_2(x) |0, 0\rangle . \tag{35}$$

This way the unitary matrix in equation 38 can be decomposed as

$$\hat{U}(x; \boldsymbol{\theta}) = \hat{U}'(\boldsymbol{\theta}) \otimes \Big(\otimes D_1(x) \otimes \hat{D}_2(x) \Big) , \tag{36}$$

where $\hat{U}'(\boldsymbol{\theta})$ does not depend on the value of x. After data encoding, we apply a number of identical quantum layers composed of beamsplitters, rotations, displacements, squeezing gates and Kerr nonlinearities. These gates are arranged in a structure similar to that prosed in [26]. **[Dani: Weight normalization]** Another important step to consider is weight normalization. Since passive photonic gates do not change the overall energy of the system, we do not apply any kind of normalization to the parameters of the passive gates. Active gates however like displacement and squeezing change the energy of the system (or photon number), and thus they can push the state into a mixed state [26], which we want to avoid as much as possible. Therefore we apply an L^2-regularization to the active weights W^{active} of the network. Therefore the loss function we use in the regression test is

$$\mathcal{L} = \frac{1}{|\mathcal{B}|} \sum_{(x,y)\in\mathcal{B}} \Big(y - \operatorname{Tr}\Big[\hat{\rho} \hat{X}_2 \Big] \Big)^2 + \frac{\lambda}{|\mathcal{B}|} \sum ||W^{\text{active}}||^2 . \tag{37}$$

where $\mathcal{B}$ is a mini-batch of size $|\mathcal{B}|$ and $\hat{\rho}$ is the otput of the quantum neural network. Some regression tasks work better if we use L^1 regularization, or even both L^1 and L^2, but we found that L^2 regularization works perfectly fine in our cases. Assuming that the output state is pure, we can write

$$\hat{\rho} = |\psi\rangle\langle\psi|, \text{ with } |\psi\rangle = \hat{U}(x; \boldsymbol{\theta}) |\psi_0\rangle . \tag{38}$$

We tested the performance of the QNN with different number of layers (see figure 9), and concluded that we need at least six layers to achieve the target MSE of 0.002 on the test set. The quantum neural network we use in the regression task is shown on figure 8.

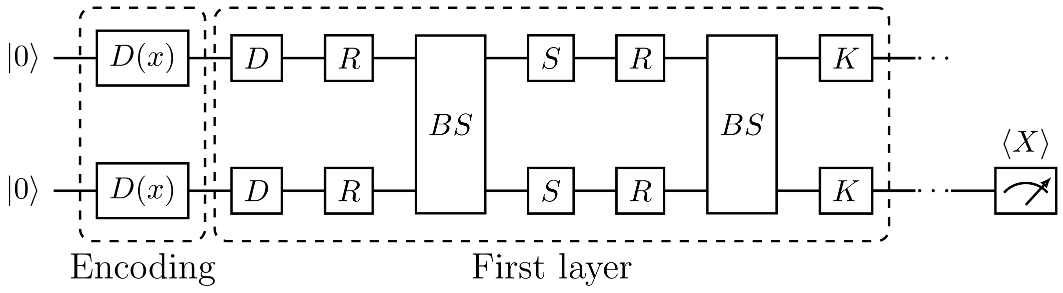

Figure 8. Ansatz circuit for the regression task. We use displacement encoding and six consecutive identical layers with a homodyne measurement at the end.

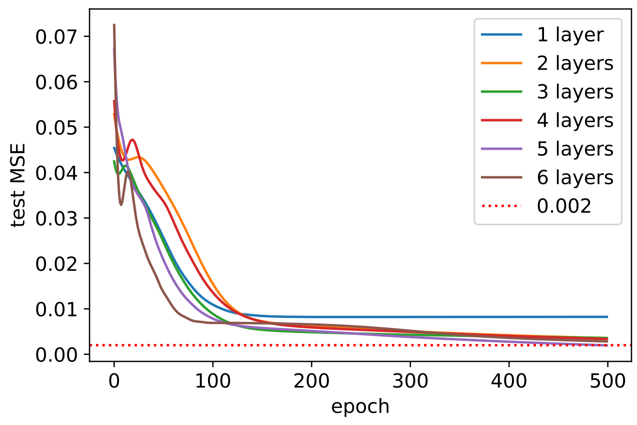

Figure 9. Comparison of the regression circuit performance on the test set with different number of layers.

We tested the quantum neural network described above on two **[Dani: three?]** datasets: one of them was a synthetic dataset, namely the $f(x) = \tanh(\pi x)$ function **[Dani: x^3?]** the other one is a normalized I-V curve of a photodiode. We run a bunch of numerical experiments experiments

	tanh	I-V
#training data	105	100
#test data	45	38
#layers	6	6
#qumodes	2	2
#shots	50 to 1000	50 to 1000
mini-batch size	4	4
λ	0.1	0.1
lr	0.001	0.001

Table 1. Hyperparameters of the regression simulations

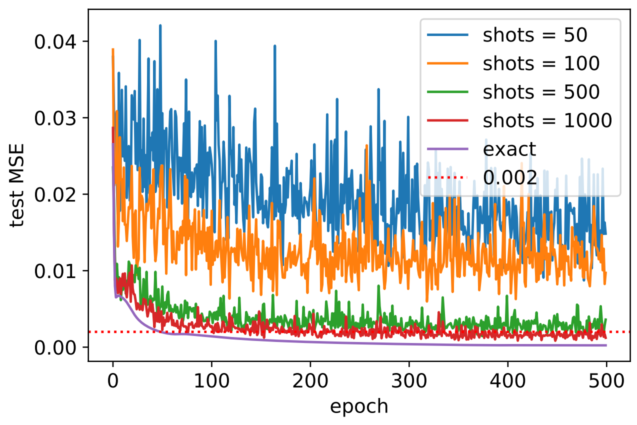

(a)

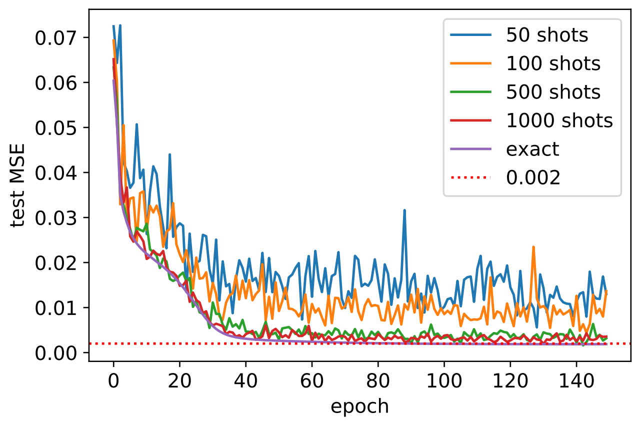

(b)

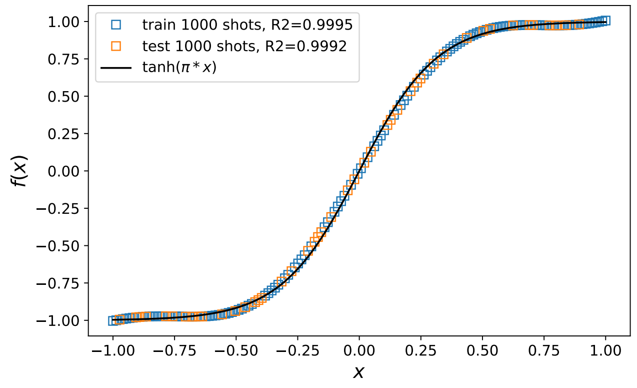

(c)

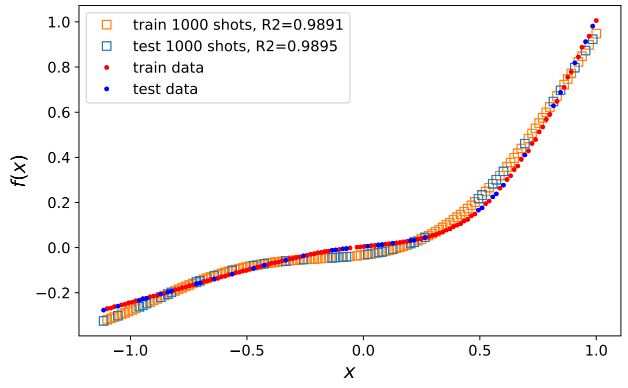

(d)

Figure 10. The top row shows how the regression circuits perform on the test set. The figures show loss curves with different number of shots for the tanh function (a) and the I-V curve (b). The bottom rows show inference tests with 1000 shots both for the tanh function (c) as well as the I-V curve (d). All simulations were run with $\alpha = 0.001$ and mini-batch size 4.

[Dani: Change tanh-results-bs=16-lr=0_001-s1000.pdf to tanh-results-bs=4-lr=0_001-s1000.pdf]

[Dani: increase tick size on inference plots]

5.3 CV-VQE for the Bose-Hubbard model

The Bose-Hubbard model introduced first by Gersch and Knollman in 1963 for the description of interacting spinless bosons on a lattice, such as ultracold bosonic atoms on an optical lattice [32, 33]. This model has also gained popularity because it is found to be an adequate model for the description of the Superfluidity-Mott insulator (SF-MI) transition, which has been experimentally demonstrated [34, 35]. We chose this model, because an exact diagonalization of the Bose-Hubbard Hamiltonian with respect to a finite dimensional Fock-basis is possible and thus the model is numerically solvable. This enables the verification of the correctness of the results given by our variational quantum solver for small problem instances.

The Bose Hubbard model which we used in our simulations is defined by the following Hamiltonian expressed with the bosonic creation and annihillation operators:

$$H = -t \sum_{i=1}^{M-1} (a_i^\dagger a_{i+1} + a_{i+1}^\dagger a_i) + \frac{U}{2} \sum_{i=1}^{M} n_i^2, \tag{39}$$

where M is the number of bosonic modes in the system. If we restrict the total number of bosons in the system to be N, the dimension of the restricted Fock-space is

$$D = \frac{(N+M-1)!}{N!(M-1)!}, \tag{40}$$

which explosively grows with the system size. Therefore finding the groundstate of the Bose-Hubbard Hamiltonian for larger systems can be intractable even on classical supercomputers, making quantum computers, especially continuous-variable quantum computers a potential candidate for solving these problems in the future. Compared to the original definition of the Bose-Hubbard Hamiltonian, we omitted the term $-\mu \sum_i^M n_i$, because it is not relevant in our particular experiments.

5.3.1 Solving the model by exact diagonalization

[Dani: Analytic solution by diagonalization] If we want to calculate the groundstate of a Bose-Hubbard model, then we need to solve the eigenvalue-problem of Hamiltonian 39. Of course a general Fock-space corresponding to a bosonic system is infinite-dimensional, therefore we have to restrict the system so that a maximum of N particles are allowed in each mode:

$$|0,0,...,0\rangle, |0,0,...,N\rangle, |0,0,...,1,N\rangle, ...|N,N,...,N\rangle.$$

Then, we can relabel the Fock-states so that each Fock basis has its own unique label j:

$$|n_{M-1}, n_{M-2}, ...n_1, n_0\rangle = \left| \sum_{k=0}^{M-1} n_k (N+1)^k \right\rangle. \tag{41}$$

This is useful, because with these relabeled states we can calculate the matrix elements of the new Hamiltonian:

$$H_{jj'} = \langle j| H |j'\rangle = \langle n_{M-1}, n_{M-2}, ...n_1, n_0 | H | n'_{M-1}, n'_{M-2}, ...n'_1, n'_0\rangle \tag{42}$$

We can further reduce the dimension of the Hilbert space if we prescribe that the total number of photons must be N:

$$\sum_k n_k = N.$$

In this case for example if the number of modes is $M = 4$ and the total number of particles is $N = 4$, the dimension of the restricted Hilbert-space is only 35.

The resulting matrix $H_{jj'}$ is usually a sparse matrix (see fig. 11), and can be diagonalized using existing software.

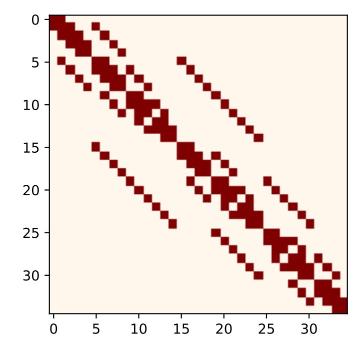
(a)

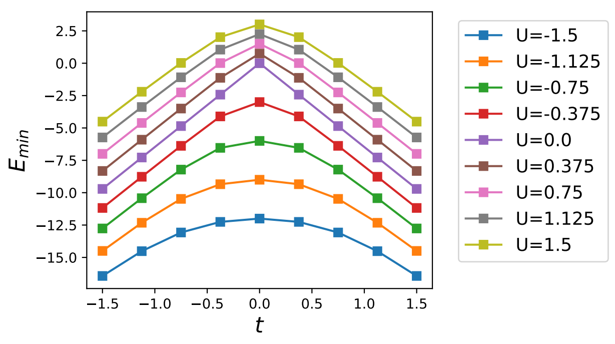

(b)

Figure 11. (a) Visual representation of a sparse Hamiltonian matrix $H_{jj'}$ for a Bose-Hubbard model with $\dim(\mathcal{H}) = 35$. Darker points show the non-zero elements in the matrix (b) Numerical solutions of the ground-state energy for different U and t values.

5.3.2 Variational solutions

VQEs introduced in section 4.1 are shown to be effective for simulating different fermionic quantum systems, like molecules or metals [20, 21, 22, 23]. In this chapter we demonstrate a photonic VQE for finding the ground-state energy of a Bose-Hubbard model. Furthermore, we show that stochastic gradient descent methods can be applied to the VQE to reduce the number of shots required, and thus reduce the overall cost of finding the ground state energy on a quantum hardware.

The variational circuit $U(\boldsymbol{\theta})$ can be realized with sequences of quantum gates, in our case photonic quantum gates. Since we want the total number of particles in the system to be preserved during the simulations, we must use photon-number preserving gates only. We composed each quantum layer from Beamsplitters, Kerr-gates and Cross-Kerr-gates (see fig. 13).

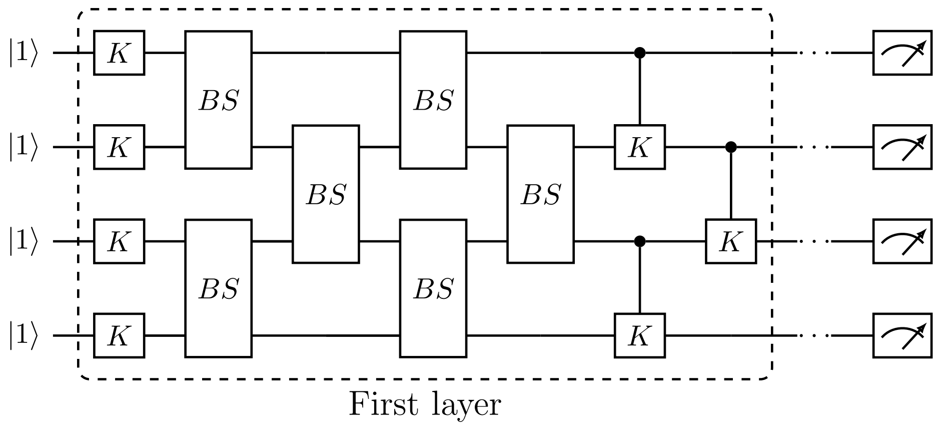

Figure 12. Illustration of a variational ansatz circuit with its first layer. Initially, each of the four qumodes contain a single photon. The layer is built up from Kerr-gates, CrossKerr gates and Beamsplitters, which are passive optical gates, so the total number of photons is preserved.

Throughout the numerical experiments, we set initially one single photon in each of the four qumodes i.e. $|\psi_0\rangle = |1\rangle^{\otimes M}$, and applied a number of identical quantum layers followed by quadrature measurements.

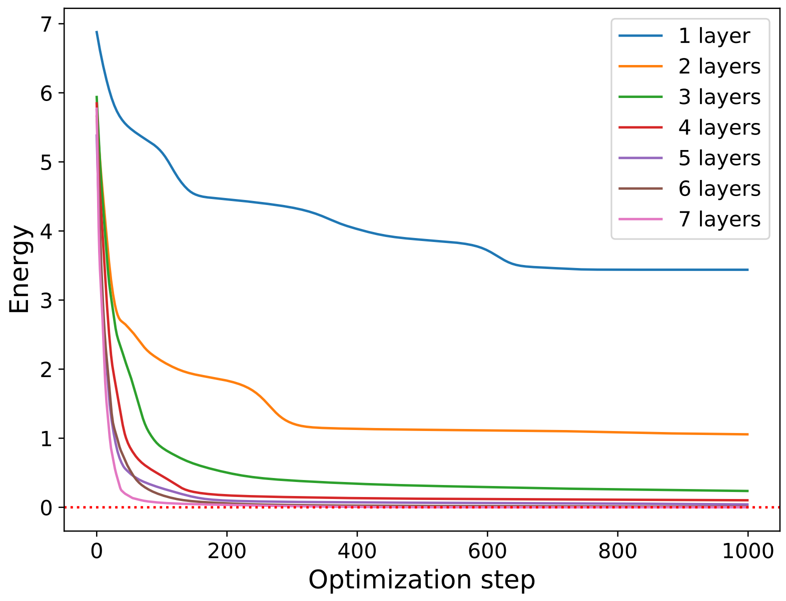

Figure 13.

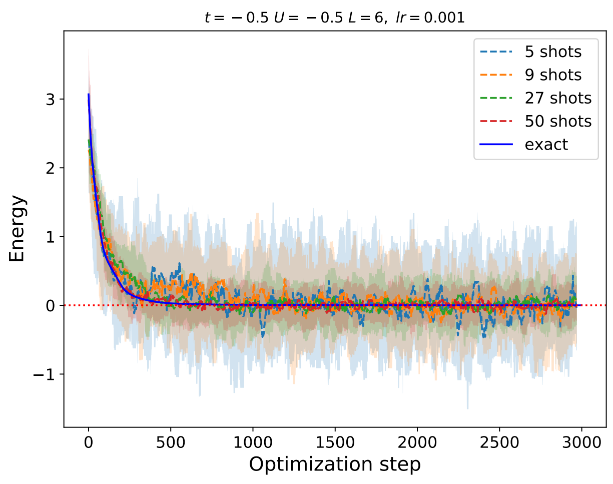

(a) first

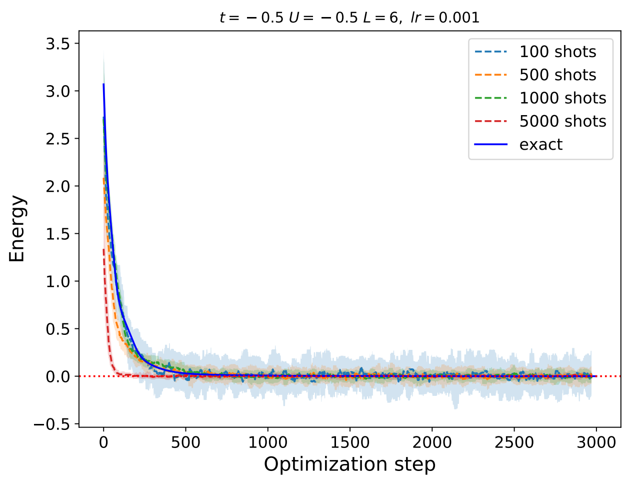

(b) second

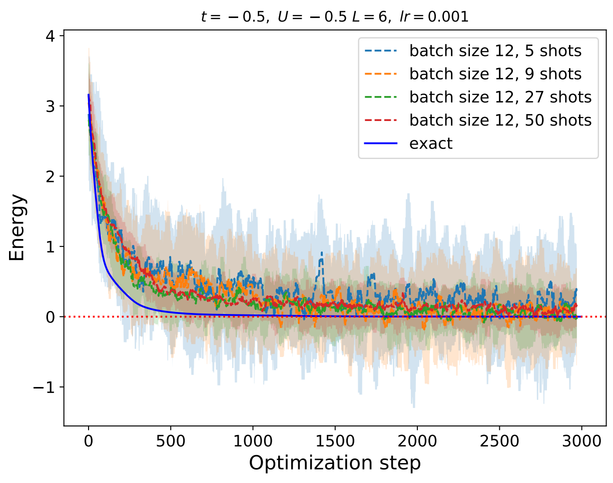

(c) third

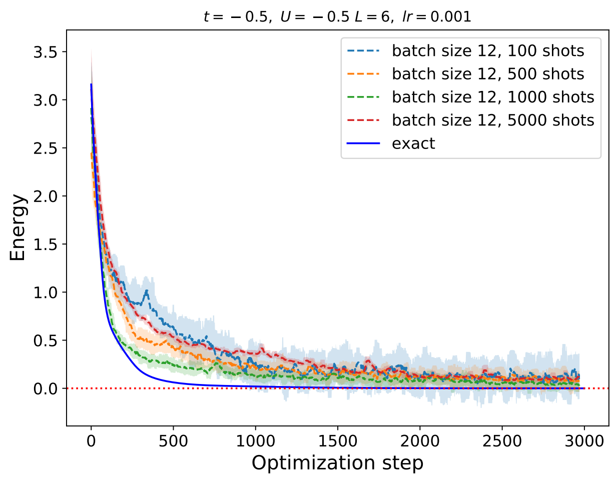

(d) fourth

Figure 14. caption

6 Conclusion and future work

References

[1] URL https://en.wikipedia.org/wiki/File:Neuron3.png.

[2] David Deutsch and Richard Jozsa. Rapid solution of problems by quantum computation. *Proceedings of the Royal Society of London. Series A: Mathematical and Physical Sciences*, 439(1907): 553–558, December 1992. doi: 10.1098/rspa.1992.0167. URL https://doi.org/10.1098/rspa.1992.0167.

[3] P.W. Shor. Algorithms for quantum computation: discrete logarithms and factoring. In *Proceedings*

35th Annual Symposium on Foundations of Computer Science. IEEE Comput. Soc. Press. doi: 10.1109/sfcs.1994.365700. URL https://doi.org/10.1109/sfcs.1994.365700.

[4] Lov K. Grover. A fast quantum mechanical algorithm for database search. In *Proceedings of the twenty-eighth annual ACM symposium on Theory of computing - STOC 1996*. ACM Press, 1996. doi: 10.1145/237814.237866. URL https://doi.org/10.1145/237814.237866.

[5] Ewin Tang. A quantum-inspired classical algorithm for recommendation systems. In *Proceedings of the 51st Annual ACM SIGACT Symposium on Theory of Computing*. ACM, June 2019. doi: 10.1145/3313276.3316310. URL https://doi.org/10.1145/3313276.3316310.

[6] Chen Ding, Tian-Yi Bao, and He-Liang Huang. Quantum-Inspired Support Vector Machine. *arXiv e-prints*, art. arXiv:1906.08902, June 2019.

[7] Juan Miguel Arrazola, Alain Delgado, Bhaskar Roy Bardhan, and Seth Lloyd. Quantum-inspired algorithms in practice. *arXiv e-prints*, art. arXiv:1905.10415, May 2019.

[8] Diederik P Kingma and Max Welling. Auto-Encoding Variational Bayes. *arXiv e-prints*, art. arXiv:1312.6114, December 2013.

[9] Volodymyr Mnih, Koray Kavukcuoglu, David Silver, Alex Graves, Ioannis Antonoglou, Daan Wierstra, and Martin Riedmiller. Playing Atari with Deep Reinforcement Learning. *arXiv e-prints*, art. arXiv:1312.5602, December 2013.

[10] David Silver, Aja Huang, Chris J. Maddison, Arthur Guez, Laurent Sifre, George van den Driessche, Julian Schrittwieser, Ioannis Antonoglou, Veda Panneershelvam, Marc Lanctot, Sander Dieleman, Dominik Grewe, John Nham, Nal Kalchbrenner, Ilya Sutskever, Timothy Lillicrap, Madeleine Leach, Koray Kavukcuoglu, Thore Graepel, and Demis Hassabis. Mastering the game of go with deep neural networks and tree search. *Nature*, 529(7587):484–489, January 2016. doi: 10.1038/nature16961. URL https://doi.org/10.1038/nature16961.

[11] Yann LeCun, Yoshua Bengio, and Geoffrey Hinton. Deep learning. *Nature*, 521(7553):436–444, May 2015. doi: 10.1038/nature14539. URL https://doi.org/10.1038/nature14539.

[12] Y. LeCun, B. Boser, J. S. Denker, D. Henderson, R. E. Howard, W. Hubbard, and L. D. Jackel. Backpropagation Applied to Handwritten Zip Code Recognition. *Neural Computation*, 1(4):541–551, 12 1989. ISSN 0899-7667. doi: 10.1162/neco.1989.1.4.541. URL https://doi.org/10.1162/neco.1989.1.4.541.

[13] Sepp Hochreiter and Jürgen Schmidhuber. Long Short-Term Memory. *Neural Computation*, 9(8): 1735–1780, 11 1997. ISSN 0899-7667. doi: 10.1162/neco.1997.9.8.1735. URL https://doi.org/10.1162/neco.1997.9.8.1735.

[14] Ashish Vaswani, Noam Shazeer, Niki Parmar, Jakob Uszkoreit, Llion Jones, Aidan N. Gomez, Lukasz Kaiser, and Illia Polosukhin. Attention is all you need. 2017. URL https://arxiv.org/pdf/1706.03762.pdf.

[15] David E. Rumelhart, Geoffrey E. Hinton, and Ronald J. Williams. Learning representations by back-propagating errors. *Nature*, 323(6088):533–536, October 1986. doi: 10.1038/323533a0. URL https://doi.org/10.1038/323533a0.

[16] Patrick Rebentrost, Masoud Mohseni, and Seth Lloyd. Quantum support vector machine for big data classification. *Phys. Rev. Lett.*, 113:130503, Sep 2014. doi: 10.1103/PhysRevLett.113.130503. URL https://link.aps.org/doi/10.1103/PhysRevLett.113.130503.

[17] Aram W. Harrow, Avinatan Hassidim, and Seth Lloyd. Quantum algorithm for linear systems of equations. *Phys. Rev. Lett.*, 103:150502, Oct 2009. doi: 10.1103/PhysRevLett.103.150502. URL https://link.aps.org/doi/10.1103/PhysRevLett.103.150502.

[18] Maria Schuld and Nathan Killoran. Quantum machine learning in feature hilbert spaces. *Phys. Rev. Lett.*, 122:040504, Feb 2019. doi: 10.1103/PhysRevLett.122.040504. URL https://link.aps.org/doi/10.1103/PhysRevLett.122.040504.

[19] Alberto Peruzzo, Jarrod McClean, Peter Shadbolt, Man-Hong Yung, Xiao-Qi Zhou, Peter J. Love, Alán Aspuru-Guzik, and Jeremy L. O'Brien. A variational eigenvalue solver on a photonic quantum processor. *Nature Communications*, 5(1), July 2014. doi: 10.1038/ncomms5213. URL https://doi.org/10.1038/ncomms5213.

[20] Shijie Wei, Hang Li, and GuiLu Long. A full quantum eigensolver for quantum chemistry simulations. *Research*, 2020:1–11, March 2020. doi: 10.34133/2020/1486935. URL https://doi.org/10.34133/2020/1486935.

[21] Frank Arute, Kunal Arya, Ryan Babbush, Dave Bacon, Joseph C. Bardin, Rami Barends, Sergio Boixo, Michael Broughton, Bob B. Buckley, David A. Buell, Brian Burkett, Nicholas Bushnell, Yu Chen, Zijun Chen, Benjamin Chiaro, Roberto Collins, William Courtney, Sean Demura, Andrew Dunsworth, Edward Farhi, Austin Fowler, Brooks Foxen, Craig Gidney, Marissa Giustina, Rob Graff, Steve Habegger, Matthew P. Harrigan, Alan Ho, Sabrina Hong, Trent Huang, William J. Huggins, Lev Ioffe, Sergei V. Isakov, Evan Jeffrey, Zhang Jiang, Cody Jones, Dvir Kafri, Kostyantyn Kechedzhi, Julian Kelly, Seon Kim, Paul V. Klimov, Alexander Korotkov, Fedor Kostritsa, David Landhuis, Pavel Laptev, Mike Lindmark, Erik Lucero, Orion Martin, John M. Martinis, Jarrod R. McClean, Matt McEwen, Anthony Megrant, Xiao Mi, Masoud Mohseni, Wojciech Mruczkiewicz, Josh Mutus, Ofer Naaman, Matthew Neeley, Charles Neill, Hartmut Neven, Murphy Yuezhen Niu, Thomas E. O'Brien, Eric Ostby, Andre Petukhov, Harald Putterman, Chris Quintana, Pedram Roushan, Nicholas C. Rubin, Daniel Sank, Kevin J. Satzinger, Vadim Smelyanskiy, Doug Strain, Kevin J. Sung, Marco Szalay, Tyler Y. Takeshita, Amit Vainsencher, Theodore White, Nathan Wiebe, Z. Jamie Yao, Ping Yeh, and Adam Zalcman. Hartree-fock on a superconducting qubit quantum computer. *Science*, 369(6507):1084–1089, 2020. ISSN 0036-8075. doi: 10.1126/science.abb9811. URL https://science.sciencemag.org/content/369/6507/1084.

[22] Abhinav Kandala, Antonio Mezzacapo, Kristan Temme, Maika Takita, Markus Brink, Jerry M. Chow, and Jay M. Gambetta. Hardware-efficient variational quantum eigensolver for small

molecules and quantum magnets. *Nature*, 549(7671):242–246, September 2017. doi: 10.1038/nature23879. URL https://doi.org/10.1038/nature23879.

[23] Cornelius Hempel, Christine Maier, Jonathan Romero, Jarrod McClean, Thomas Monz, Heng Shen, Petar Jurcevic, Ben P. Lanyon, Peter Love, Ryan Babbush, Alán Aspuru-Guzik, Rainer Blatt, and Christian F. Roos. Quantum chemistry calculations on a trapped-ion quantum simulator. *Phys. Rev. X*, 8:031022, Jul 2018. doi: 10.1103/PhysRevX.8.031022. URL https://link.aps.org/doi/10.1103/PhysRevX.8.031022.

[24] D. Zhu, N. M. Linke, M. Benedetti, K. A. Landsman, N. H. Nguyen, C. H. Alderete, A. Perdomo-Ortiz, N. Korda, A. Garfoot, C. Brecque, L. Egan, O. Perdomo, and C. Monroe. Training of quantum circuits on a hybrid quantum computer. *Science Advances*, 5(10):eaaw9918, October 2019. doi: 10.1126/sciadv.aaw9918. URL https://doi.org/10.1126/sciadv.aaw9918.

[25] Diederik P. Kingma and Jimmy Ba. Adam: A method for stochastic optimization. *CoRR*, abs/1412.6980, 2015.

[26] Nathan Killoran, Thomas R. Bromley, Juan Miguel Arrazola, Maria Schuld, Nicolás Quesada, and Seth Lloyd. Continuous-variable quantum neural networks. *Phys. Rev. Research*, 1:033063, Oct 2019. doi: 10.1103/PhysRevResearch.1.033063. URL https://link.aps.org/doi/10.1103/PhysRevResearch.1.033063.

[27] Maria Schuld, Ville Bergholm, Christian Gogolin, Josh Izaac, and Nathan Killoran. Evaluating analytic gradients on quantum hardware. *Phys. Rev. A*, 99:032331, Mar 2019. doi: 10.1103/PhysRevA.99.032331. URL https://link.aps.org/doi/10.1103/PhysRevA.99.032331.

[28] Nathan Killoran, Josh Izaac, Nicolás Quesada, Ville Bergholm, Matthew Amy, and Christian Weedbrook. Strawberry Fields: A Software Platform for Photonic Quantum Computing. *Quantum*, 3:129, March 2019. ISSN 2521-327X. doi: 10.22331/q-2019-03-11-129. URL https://doi.org/10.22331/q-2019-03-11-129.

[29] Thomas R. Bromley, Juan Miguel Arrazola, Soran Jahangiri, Josh Izaac, Nicolás Quesada, Alain Delgado Gran, Maria Schuld, Jeremy Swinarton, Zeid Zabaneh, and Nathan Killoran. Applications of near-term photonic quantum computers: software and algorithms. *Quantum Science and Technology*, 5(3):034010, July 2020. doi: 10.1088/2058-9565/ab8504.

[30] Martín Abadi, Paul Barham, Jianmin Chen, Zhifeng Chen, Andy Davis, Jeffrey Dean, Matthieu Devin, Sanjay Ghemawat, Geoffrey Irving, Michael Isard, et al. Tensorflow: A system for large-scale machine learning. In *12th {USENIX} Symposium on Operating Systems Design and Implementation ({OSDI} 16)*, pages 265–283, 2016.

[31] F. Pedregosa, G. Varoquaux, A. Gramfort, V. Michel, B. Thirion, O. Grisel, M. Blondel, P. Prettenhofer, R. Weiss, V. Dubourg, J. Vanderplas, A. Passos, D. Cournapeau, M. Brucher, M. Perrot, and E. Duchesnay. Scikit-learn: Machine learning in Python. *Journal of Machine Learning Research*, 12:2825–2830, 2011.

[32] H. A. Gersch and G. C. Knollman. Quantum cell model for bosons. *Phys. Rev.*, 129:959–967, Jan 1963. doi: 10.1103/PhysRev.129.959. URL https://link.aps.org/doi/10.1103/PhysRev.129.959.

[33] D. Jaksch and P. Zoller. The cold atom Hubbard toolbox. *Annals of Physics*, 315(1):52–79, January 2005. doi: 10.1016/j.aop.2004.09.010.

[34] D. Jaksch, C. Bruder, J. I. Cirac, C. W. Gardiner, and P. Zoller. Cold bosonic atoms in optical lattices. *Phys. Rev. Lett.*, 81:3108–3111, Oct 1998. doi: 10.1103/PhysRevLett.81.3108. URL https://link.aps.org/doi/10.1103/PhysRevLett.81.3108.

[35] Markus Greiner, Olaf Mandel, Tilman Esslinger, Theodor W. Hänsch, and Immanuel Bloch. Quantum phase transition from a superfluid to a mott insulator in a gas of ultracold atoms. *Nature*, 415 (6867):39–44, January 2002. doi: 10.1038/415039a. URL https://doi.org/10.1038/415039a.

A Coherent states

A coherent state is the eigenstate of $\hat{a}$:

$$\hat{a}\left|\alpha\right\rangle = \alpha\left|\alpha\right\rangle$$

$$\left|\alpha\right\rangle = \sum_{n=0}^{\infty}\left|n\right\rangle\left\langle n|\alpha\right\rangle$$

we have

$$\hat{a}\left|\alpha\right\rangle = \alpha\left|\alpha\right\rangle \implies \left\langle n|\hat{a}|\alpha\right\rangle = \alpha\left\langle n|\alpha\right\rangle$$

and

$$\begin{aligned} \hat{a}^{\dagger}\left|n\right\rangle = \sqrt{n+1}\left|n+1\right\rangle &\implies \left\langle n\right|\hat{a} = \sqrt{n+1}\left\langle n+1\right| \\ \implies \left\langle n|\hat{a}|\alpha\right\rangle &= \sqrt{n+1}\left\langle n+1|\alpha\right\rangle = \alpha\left\langle n|\alpha\right\rangle \\ \implies \left\langle n|\alpha\right\rangle &= \frac{\alpha}{\sqrt{n}}\left\langle n-1|\alpha\right\rangle = \cdots = \frac{\alpha^n}{\sqrt{n!}}\left\langle 0|\alpha\right\rangle \end{aligned}$$

therefore,

$$\left|\alpha\right\rangle = \sum_{n=0}^{\infty}\frac{\alpha^n}{\sqrt{n!}}\left\langle 0|\alpha\right\rangle\left|n\right\rangle$$

, The value of $\langle 0|\alpha\rangle$ can be calculated from the normalization condition $\langle\alpha|\alpha\rangle \overset{!}{=} 1$. Since

$$\begin{aligned} |\alpha\rangle &= \langle 0|\alpha\rangle \sum_{n=0}^{\infty} \frac{\alpha^n}{\sqrt{n!}} |n\rangle \\ \langle\alpha| &= \langle\alpha|0\rangle \sum_{k=0}^{\infty} \frac{(\alpha^*)^k}{\sqrt{k!}} \langle k| , \end{aligned}$$

we have

$$\begin{aligned} 1 \overset{!}{=} \langle\alpha|\alpha\rangle &= \left(\langle\alpha|0\rangle \sum_{k=0}^{\infty} \frac{(\alpha^*)^k}{\sqrt{k!}} \langle k|\right)\left(\langle 0|\alpha\rangle \sum_{n=0}^{\infty} \frac{\alpha^n}{\sqrt{n!}} |n\rangle\right) \\ &= \langle\alpha|0\rangle \langle 0|\alpha\rangle \sum_{k=0}^{\infty}\sum_{n=0}^{\infty} \frac{(\alpha^*)^k\alpha^n}{\sqrt{k!n!}} \langle k|n\rangle \\ &= \langle\alpha|0\rangle \langle 0|\alpha\rangle \sum_{k=0}^{\infty}\sum_{n=0}^{\infty} \frac{(\alpha^*)^k\alpha^n}{\sqrt{k!n!}} \delta_{kn} \\ &= |\langle 0|\alpha\rangle|^2 \sum_{n=0}^{\infty} \frac{(|\alpha|^2)^n}{n!} = |\langle 0|\alpha\rangle|^2 e^{|\alpha|^2}. \end{aligned}$$

$$\implies \langle 0|\alpha\rangle = e^{i\varphi} e^{-\frac{|\alpha|^2}{2}}$$

And so, a coherent state can be written as

$$|\alpha\rangle = e^{i\varphi} e^{\frac{-|\alpha|^2}{2}} \sum_{n=0}^{\infty} \frac{\alpha^n}{\sqrt{n!}} |n\rangle$$

B Mathematical preliminaries

B.1 Hilbert spaces

Definition 1. ***Hilbert-space***
Given a field T (real or complex), a vector space $\mathcal{H}$ endowed with an inner product, is called a Hilbert-space, if it is a complete metric space with respect to the distance function induced by the inner product. The inner product is a map $\langle\cdot|\cdot\rangle : \mathcal{H} \times \mathcal{H} \to T$, for which $\forall x, y, z \in \mathcal{H}$:

- $\langle x|x\rangle \geq 0$
- $\langle x|x\rangle = 0 \iff x = \mathbf{0} \in \mathcal{H}$
- $\langle x|y\rangle = \langle y|x\rangle^*$, *where * denotes complex conjugation.*
- $\langle x|\alpha y + \beta z\rangle = \alpha \langle x|y\rangle + \beta \langle x|z\rangle$, *where $\alpha, \beta \in T$*

The norm induced by this inner product is a map $||\cdot|| : \mathcal{H} \to T$ defined as

$$||x|| = \sqrt{\langle x|x\rangle},$$

And the metric induced by this norm is defined as

$$d(x,y) = ||x-y|| = \sqrt{\langle x-y|x-y\rangle}.$$

The space $\mathcal{H}$ is said to be complete if every Cauchy-sequence is convergent with respect to the norm, and the limit is in $\mathcal{H}$. That is, each sequence $x_1, x_2, \ldots$, for which

$$\forall \varepsilon > 0\ \exists N(\varepsilon) \text{ so, that } n > m > N(\varepsilon) \implies ||x_n - x_m|| < \varepsilon.$$

Definition 2. ***Linear functional***
Let $\mathcal{H}$ be a Hilbert-space over the field T. Then, the map $\varphi : \mathcal{H} \to T$ is called a linear functional, if

$$\varphi(\alpha x + \beta y) = \alpha\varphi(x) + \beta\varphi(y),\ \forall \alpha, \beta \in T,\ x, y \in \mathcal{H}.$$

Definition 3. ***Dual space***
Given a Hilbert-space $\mathcal{H}$, its dual space, $\mathcal{H}^*$ is the space of all continuous linear functionals from the space H into the base field. The norm of an element in $\mathcal{H}^*$ is

$$||\varphi||_{\mathcal{H}^*} \overset{def}{=} \sup_{||x||=1,\, x\in\mathcal{H}} |\varphi(x)|.$$

Theorem 1. ***Riesz representation theorem***
For every element $y \in \mathcal{H}$, there exists a unique element $\varphi_y \in \mathcal{H}^*$, defined by

$$\varphi_y(x) = \langle y|x\rangle,\ \forall x \in \mathcal{H}.$$

The mapping $y \mapsto \varphi_y$ is an antilinear mapping i.e. $\alpha y_1 + \beta y_2 \mapsto \alpha^*\varphi_{y_1} + \beta^*\varphi_{y_2}$, and the Riesz-representation theorem states that this mapping is an antilinear isomorphism. The inner product in $\mathcal{H}^*$ satisfies

$$\langle \varphi_x|\varphi_y\rangle = \langle x|y\rangle^* = \langle y|x\rangle.$$

Moreover, $||y||_{\mathcal{H}} = ||\varphi_y||_{\mathcal{H}^*}$.

Definition 4. ***Dirac-notation***
From now on, the elements in $\mathcal{H}$ will be denoted by $|x\rangle$ and their corresponding element in $\mathcal{H}^*$ as $\langle x|$.

B.2 Linear operators on Hilbert spaces

Definition 5. ***Linear operators***
A map $\hat{A}:\mathcal{H}_1\to\mathcal{H}_2$ is a linear operator, if

$$\hat{A}(\alpha\,|x\rangle+\beta\,|y\rangle)=\alpha(\hat{A}\,|x\rangle)+\beta(\hat{A}\,|y\rangle).$$

Remark 1. *If not stated otherwise, we will assume that $\mathcal{H}_1=\mathcal{H}_2=\mathcal{H}$.*

Remark 2. *Operators will be denoted with a hat $(\hat{\cdot})$.*

Definition 6. ***Bounded linear operators***
A linear operator $\hat{A}:\mathcal{H}\to\mathcal{H}$ is bounded, if

$$\exists m\in\mathbb{R}:|\,\langle v|\hat{A}|v\rangle\,|\leq m\,\langle v|v\rangle\,,\,\forall\,|v\rangle\in\mathcal{H}$$

Remark 3. *The set of all bounded operators on $\mathcal{H}$ is denoted $\mathcal{B}(\mathcal{H})$.*

Definition 7. ***Commutators and anticommutators***
Since operators usually do not commute, its useful to define their commutator and anticommutator:

$$[\hat{A},\hat{B}]=\hat{A}\hat{B}-\hat{B}\hat{A}$$
$$\{\hat{A},\hat{B}\}=\hat{A}\hat{B}+\hat{B}\hat{A}$$

Definition 8. ***Operator norm***
The operator norm of an operator $\hat{A}$ is defined as

$$||\hat{A}||\overset{def}{=}\inf\{c\geq 0:||\hat{A}\,|v\rangle\,||\leq c||\,|v\rangle\,||,\,\forall\,|v\rangle\in\mathcal{H}\}$$

Definition 9. ***Trace-class operators***
An operator $\hat{A}$ is called trace-class if it admits a well defined and finite trace $\mathrm{Tr}\left[\hat{A}\right]=\sum_j\langle j|\hat{A}|j\rangle$

Definition 10. ***Positive operators***
An operator $\hat{A}$ is called positive if $\langle v|\hat{A}|v\rangle\geq 0,\forall\,|v\rangle\in\mathcal{H}$. If $\hat{A}=\sum_j\lambda_j\,|j\rangle\,\langle j|$ then $\hat{A}$ is positive if $\lambda_j\geq 0$.

Definition 11. ***Projections*** *An operator $\Pi:\mathcal{H}\to\mathcal{H}$ is a projection if* $\Pi^2=\Pi$.

B.3 Hermitian Operators, Unitary Operators, Spectral theorem, Hadamard-lemma

Definition 12. ***Hermitian adjoint***
Consider a **bounded** *linear operator $\hat{A}:\mathcal{H}\to\mathcal{H}$. The hermitian adjoint of $\hat{A}$ is a bounded linear*

operator $\hat{A}^\dagger : \mathcal{H} \to \mathcal{H}$ which satisfies

$$\langle y| \hat{A} |x\rangle = \left(\langle x| \hat{A}^\dagger |y\rangle\right)^*, \ \forall |x\rangle, |y\rangle \in \mathcal{H}. \tag{43}$$

Definition 13. ***Hermitian operators***
A bounded linear operator $\hat{H} : \mathcal{H} \to \mathcal{H}$ is Hermitian if

$$\hat{H} = \hat{H}^\dagger, \ \textit{i.e.}\ \hat{H} |x\rangle = \hat{H}^\dagger |x\rangle, \ \forall |x\rangle \in \mathcal{H}. \tag{44}$$

Definition 14. ***Unitary operator***
A bounded linear operator $\hat{U} : \mathcal{H} \to \mathcal{H}$ is unitary if

$$\hat{U}\hat{U}^\dagger = \hat{U}^\dagger\hat{U} = 1, \ \textit{in other words, } \hat{U}^\dagger = \hat{U}^{-1}. \tag{45}$$

Definition 15. ***Eigenvalues and eigenvectors***
Consider bounded linear operator $\hat{A}$. If exist a vectors $|k\rangle \in \mathcal{H}$ such that

$$\hat{A} |k\rangle = \lambda_k |k\rangle, \tag{46}$$

then $|k\rangle$ is called an eigenvector of $\hat{A}$ and λk is the corresponding eigenvalue.

An important property of Hermitian operators is that they can be diagonalized with real eigenvalues. This is formally stated by the spectral theorem:

Theorem 2. ***The Spectral theorem***
Let $\hat{A}$ be a bounded Hermitian operator on some Hilbert-space $\mathcal{H}$. Then there exists an orthonormal basis in $\mathcal{H}$ which consists of the eigenvectors of $\hat{A}$ and each eigenvalue of $\hat{A}$ is real.

This means that any bounded Hermitian operator $\hat{H}$ can be decomposed as

$$\hat{H} = \sum_k \lambda_k \hat{P}_k = \sum_k \lambda_k |k\rangle\langle k| \tag{47}$$

where λ_k and $|k\rangle$ are the eigenvalues and eigenvectors of $\hat{H}$.

Definition 16. ***Exponential of operators*** *If X is a linear operator, we can define the exponential of X:*

$$e^X = \sum_{n=0}^{\infty} \frac{X^n}{n!}$$

Important: The product of exponentials of operators generally isn't equal to the exponential of their sum:

$$e^X e^Y = e^{Z(X,Y)} \neq e^{X+Y},$$

where $Z(X,Y)$ is given by the Baker-Campbell-Hausdorff formula:

$$Z(X,Y) = X + Y + \frac{1}{2}[X,Y] + \frac{1}{12}[X,[X,Y]] - \frac{1}{12}[Y,[X,Y]] - \frac{1}{24}[Y,[X,[X,Y]]] \\ - \frac{1}{720}([[[[X,Y],Y],Y],Y] + [[[Y,X],X],X],X]) + ...$$

It is however equal if $[X,Y]=0$:

$$\text{if}\,[X,Y] = 0 \implies e^X e^Y = e^{X+Y}$$

There are 2 important special cases:

Theorem 3. ***The Hadamard-lemma***

$$e^X Y e^{-X} = Y + [X,Y] + \frac{1}{2!}[X,[X,Y]] + \frac{1}{3!}[X,[X,[X,Y]]] + ...$$

Theorem 4. *If X and Y commute with their commutator, i.e. $[X,[X,Y]] = [Y,[X,Y]] = 0$, then:*

$$e^X e^Y = e^{X+Y+\frac{1}{2}[X,Y]}$$

Theorem 5. *If $[X,Y] = sY$ with $s \in \mathbb{C}, s \neq 2i\pi n, n \in \mathbb{Z}$ then:*

$$e^X e^Y = \exp\left(X + \frac{s}{1-e^{-s}}Y\right)$$

B.4 Pure and mixed quantum states

Definition 17. ***Quantum states***
A quantum state of a quantum system is a mathematical entity that provides a probability distribution for the outcomes of each possible measurement on the system.

Definition 18. ***Pure quantum states***
Pure quantum states are quantum states that can be described by a vector $|\psi\rangle$ of norm 1.

If one multiplies a pure quantum state by a complex scalar $e^{i\alpha}$, then the new state is physically equivalent to the former, thus $|\psi\rangle$ and $e^{i\alpha}|\psi\rangle$ are the same pure state. The transformation $|\psi\rangle \to e^{i\alpha}|\psi\rangle$ does not change the outcomes of measurements on the state, however the phase α is important in quantum algorithms.

Example. *For example, the states $\frac{1}{\sqrt{2}}(|0\rangle + e^{i\pi}|1\rangle)$ and $\frac{1}{\sqrt{2}}(|0\rangle + e^{i\frac{\pi}{2}}|1\rangle)$ are not the same quantum state, but in both states there is 50-50 percent probability of measuring $|0\rangle$ and $|1\rangle$.*

Definition 19. ***Density Matrix***
A quantum state $\hat{\rho}$ is a trace-1, self-adjoint, positive semidefinite operator. The set of quantum states is

$$\mathcal{S}(\mathcal{H}) = \{\hat{\rho} : \hat{\rho} \geq 0, \hat{\rho} = \hat{\rho}^\dagger, \mathrm{Tr}\,[\hat{\rho}] = 1\}$$

A quantum state is pure if and only if $\hat{\rho}^2 = \hat{\rho}$*. Also, if* ρ *is a pure state, then it can be written as* $\hat{\rho} = |\psi\rangle\langle\psi|$*. The operator* ρ *is called the density operator or density matrix.*